Negatively Buoyant Jet (or Plume) with Applications to Snowplow Exit Flow Behavior

WILLIAM R. LINDBERG AND JOSEPH D. PETERSEN

The initial findings of an ongoing study of negatively buoyant jet (or plume) behavior are described. The motivation for this research is to quantify the dynamics of the exit snow plume from displacement and rotary snow plows. The effects of injection angle and cross flow on the jet (or plume) behavior were of particular interest in this phase of the study. A water tow tank was used for the experiments, in which the exit jet was towed through quiescent water at a constant velocity. Photographic records of the jet (or plume) structure were used to measure the jet (or plume) dimensions. Dimensional reasoning yielded a set of dimensionless parameters that correlated the jet or plume length scales over a wide range of the experimental parameters. Three flow regimes have been identified, which depend on the Froude number, F_0, of the cross flow: $F_0 << 1$, negligible cross flow; $0 < F_0 < 1$, weak cross flow; and $F_0 > 1$, strong cross flow; where $F_0 = U_0/(g_0')^{1/2}$, U_0 is the cross-flow velocity, g' is the reduced gravity, and r_0 is the jet radius. Correlations of the measured length scales with F_0 were determined for all three flow regimes.

An important aspect of the performance of snowplows is the behavior of the snow after it exits from the moldboard. The exiting snow experiences a different dynamic environment from the flow conditions along the moldboard itself. At the exit plane, the flow has acquired considerable momentum in the transverse direction (i.e., normal to the plow motion). The flow then persists as a free jet whose trajectory depends on this momentum and the modifying external forces. The forces on this exit fluid include gravity and a complex three-dimensional interaction with the surrounding air, in the forms of entrainment and drag.

Knowledge of the exit plume flow for a variety of operational conditions is viewed as an important element in understanding plow performance, including cast distances, plume trajectories and dilutions, visibility, and the potential for altering these characteristics by plow design and operator control.

Little prior work applicable to exit plume behavior has been reported. In order to begin to address this shortcoming, a laboratory program was initiated to systematically examine the characteristics of negatively buoyant jet (or plumes) subjected to cross flows. A fundamental approach to this study has been adopted, in which the full complexity of the problem is initially reduced to allow focus on the basic flow phenomena. Additional parameters may then be introduced and their effects placed in the context of previous observations.

Department of Mechanical Engineering, University of Wyoming, Laramie, Wyo. 82071.

BACKGROUND

The wide variety of circumstances occurring for the behavior of a jet (or plume) whose density is different from its surroundings has stimulated research on this topic for decades. The majority of this work has centered on the positively buoyant case, for which the density increment of the jet (or plume) provides a body force in the same general direction as the initial injection direction (i.e., a light fluid injected upward, or a heavy fluid injected downward). Examples of a positively buoyant jet (or plume) include a cumulus cloud, an industrial smokestack, and the rising column of smoke from a campfire.

A negatively buoyant jet (or plume) has a body force in the opposite direction from the vertical component of the injection velocity. In this case, equilibrium heights or flow reversals are always present. The term "vertical component of the injection velocity" is used because these jets can be aligned at an angle to the vertical. Examples of this type of flow other than the behavior of a plume of snow particles after exiting from a snowplow blade include the vertical injection of a dense gas into the atmosphere and the introduction of saline water into a lake or river.

A distinction can be made between a jet and a plume. A jet is a flow caused by a source of concentrated momentum such as the flow induced by the discharge from a pipe or orifice. The driving force for a plume is the downward body force or upward buoyancy of the plume itself. As an example, an initially positively buoyant jet in a stream expands, slows down, and dilutes with increasing downstream distance. Eventually, the momentum of the fluid decreases to the same order as that caused by the buoyancy. As buoyancy begins to dominate the flow dynamics, the jet becomes plume-like and behaves differently. The same processes are present for a negatively buoyant jet (or plume), with the distinction of the reversed body force for the plume, which retards and ultimately reverses the vertical motion.

The presence of an ambient cross flow further complicates this process. This external flow can have the effect of turning the jet (or plume) flow toward the downstream direction and will also alter the internal flow behavior of the jet (or plume) itself.

Laboratory studies of turbulent jets and plumes have been useful in applications in which the prototype and laboratory scales are considerably different. Dimensional and dynamic similarity arguments are insufficient to justify this success without the underlying premise of Reynolds number independence in these turbulent shear flows. It has been observed

that the large-scale turbulent motions are dynamically similar for flows with widely differing Reynolds numbers. The large-scale motions dominate such processes as entrainment, momentum transfer, and mixing. All of these processes are central to the dynamical behavior of jets and plumes. Laboratory studies in which the basic shear flow is turbulent may then be used to stimulate flows whose Reynolds numbers are different, but whose basic behavior is similar.

A dimensional analysis of jets and plumes may be performed to identify the basic parameters of these flows. Figure 1 shows a schematic of the geometry of the negatively buoyant jet (or plume) in an ambient flow. The jet of density ρ_j exits the nozzle of radius r_0 at a velocity of U_j into ambient fluid surroundings of density ρ_a. The ambient flow velocity is U_0. The axis of the jet is inclined an angle θ from the horizontal in a plane perpendicular to the ambient flow direction.

The two most important dynamical parameters of the initial jet are the jet momentum M and buoyancy B fluxes (normalized with jet exit density):

$$M = \pi r_0^2 U_j^2$$

$$B = \pi r_0^2 U_j[(\rho_j - \rho_a)/\rho_j]g$$

where g is the gravitational acceleration.

The desired observable geometric parameters include $\mathbf{X}_m$, $\mathbf{W}_m$, $\mathbf{X}_t$ and $\boldsymbol{\alpha}$ where $\mathbf{X}_m$ is the (x,y,z) length scale triad when the jet is at its maximum height, $\mathbf{W}_m$ is the jet width (W_y,W_z) at the same location, $\mathbf{X}_t$ is the $x,y)$ length scale for the return of the jet (or plume) centerline to the original height of the jet, and $\boldsymbol{\alpha}$ is the spread-rate parameter (dW_y/ds, dW_z/ds, where s is directed along the jet or plume) centerline. Dynamic parameters such as velocity scales and dilution rates are also of importance but have not been measured in these studies.

Dimensional analysis, using the defined parameters, yields the following functional set of dimensionless parameters:

$$\mathbf{L}^* = F_j\mathbf{f}(F_0,\mathrm{Re}_j,\theta) \tag{1}$$

where

$\mathbf{L}^* = \mathbf{L}/r_0$ (or α),
$\mathbf{L}$ = dimensional length scale (i.e., $\mathbf{X}_m$, $\mathbf{W}_m$, or $\mathbf{X}_t$),
$F_j = U_j/[g'r_0]^{1/2}$ (the jet Froude number),
$F_0 = U_0/[g'r_0]^{1/2}$ (the cross-flow Froude number),
$\mathrm{Re}_j = 2U_jr_0/\nu$ (the jet Reynolds number),
$g' = [(\rho_j - \rho_a)/\rho_j]g$ (the reduced gravity), and
ν = kinematic viscosity.

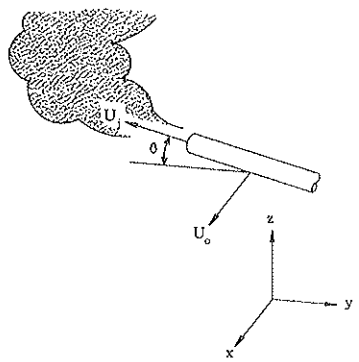

FIGURE 1 Basic geometry of the negatively buoyant jet (or plume) that is translating relative to the ambient fluid.

The assumption of Reynolds number independence for sufficiently large $\mathrm{Re}_j(\mathrm{Re} \gtrsim 500)$, reduces the number of independent parameters to three: F_j, F_0, and θ:

$$\mathbf{L}^* = F_j\mathbf{f}(F_0,\theta) \tag{2}$$

All the experimental data are presented in this form.

Three vertical length scales for this flow may be identified (*1,2*). These length scales are based on the vertical scale where there is a dynamical balance of the various forces acting on the jet or plume:

$$l_b = (M \sin\theta)^{3/4}/B^{1/2}$$

$$l_m = M^{1/2}\sin\theta/U_0$$

$$l_p = B\sin\theta/U_0^3 \tag{3}$$

These length scales represent the vertical transition points between various modes of the jet or plume behavior:

$z \sim l_b$ jet-plume transition (for negligible ambient flow),

$z \sim l_m$ transition point for bent-over jet in an ambient flow, and

$z \sim l_p$ transition point for bent-over plume in an ambient flow.

Not all of these length scales are independent, for example:

$$F_0 \sim (l_b/l_p)^{1/3} \sim (l_b/l_m) \tag{4}$$

The effect of the ambient crossflow may then be characterized in terms of the magnitude of F_0, as follows: $F_0 << 1$, negligible cross flow; $F_0 < 1$, weak cross flow; and $F_0 > 1$, strong cross flow.

In addition, the ratio of l_b to r_0 is proportional to F_j:

$$l_b/r_0 = (\pi\sin\theta)^{3/4}F_j \tag{5}$$

Because there is a transition region of approximately 10 jet diameters for the basic jet shear flow to develop, small values of F_j would indicate that the flow was still developing when the buoyancy forces were beginning to be important. Low values of F_j were avoided.

At this point, it is appropriate to point out those parameters that have not been included in this study. The four most important parameters are the crossflow Reynolds number, Re_0; the fluid density ratio, S_ρ; the azimuthal jet angle in a vertical plane relative to the plane normal to the crossflow direction (identical to a spherical coordinate system), ϕ; and the nozzle geometry.

$$\mathrm{Re}_0 = U_0l_s/\nu$$

$$S_\rho = \rho_j/\rho_a$$

where l_s is the transverse length scale of the jet or plume.

Studies have clearly shown that cross flows directly alter the internal dynamics of jet or plume flows, but the resulting flow behavior is relatively insensitive to variations in Re_0, provided Re_0 is sufficiently large.

For the present experiments, the flow is approximately Boussinesq [i.e. $S_\rho \sim O(1)$], so these experimental results should be adequately molded without the inclusion of S_ρ as an independent parameter. The density ratio is incorporated in the buoyancy flux parameter, B, as it has been defined, which does reflect non-Boussinesq effects.

This study was intended to provide the benchmarks for comparison to other studies incorporating such effects as large density ratios, azimuthal injection angles, and noncircular exit jet geometries. At present, the importance of these effects remains unresolved.

RELATED STUDIES

A limited amount of study of snowplow plume behavior has been performed. As has been pointed out by Minsk (*3*), the cast distance (Y_{max}) for a snowplow has historically been modeled by equations of the form

$$Y^* = \eta_d g(\theta,\phi)\ (\eta F_0)^2 \tag{6}$$

where

η_d = dynamic efficiency,
$g(\theta,\phi)$ = sin 2θ sin ϕ, and
η = moldboard efficiency ($\sim U_j/U_0$).

This functional form of the cast distance has its theoretical origin in simple particle trajectory analysis. The effects of drag, entrainment, turbulence, and density are accounted for in the dynamic efficiency parameter, η_d. For example, Vinnicombe (*4*) reports η_d to range from 0.53 to 0.68. Shalman (*5*) cites the following form for η_d:

$$\eta_d = \tanh\ [a_0(H\rho_s)^{1/2}] \tag{7}$$

where

a_0 = 6.2 (cm^3/g-m)$^{1/2}$,
H = undisturbed snow depth (m), and
ρ_s = undisturbed snow density (g/cm^3).

Such a formulation is probably most appropriate for wet, cohesive snow, where the plume entrains little, if any, surrounding air, similar to the behavior of a water jet. The appropriateness and limitations of this type of approach are not at present resolved.

In contrast, an exit plume composed of dry, cohesionless snow will behave as a heavy fluid, characterized by strong entrainment, drag, and mixing with the surrounding fluid. It is this situation that is most appropriately modeled by the approach of the present research.

The fluid dynamical modeling of snow avalanche motion using water tanks has been discussed by Hopfinger and Beghin (*6*) and Hopfinger (*7*). They were successful in properly scaling many of the observed features of avalanche behavior in the laboratory. The non-Boussinesq effects of $S_\rho > 1$ were examined and found to be relatively minor up to $S_\rho \sim 10$.

Studies of negatively buoyant jet or plumes are quite limited. In particular, only a few laboratory studies of these flows have been reported (*8–16*).

An experimental study of a vertically injected dense jet in a water tank was reported by Turner (*9*), for the case of 0 cross flow. Unfortunately, Turner incorrectly reported his correlated results, and the error has been propagating in the literature since that time. The correct result for the maximum rise height of the vertically injected dense fluid is

$$Z^*_{max} = 4.17\ F_j \tag{8}$$

This result is consistent with the dimensional arguments of Equation 2.

The work of Hoot et al. (*12,13,17*) is of particular significance, both in its scope and in the quality of the experimental measurements. They report on wind tunnel studies of dense gases injected vertically in a low turbulence flow. Their quiescent flow studies were in complete agreement with Equation 6. Density ratios, S_ρ of between 1.5 and 3 were used. An integral analysis for the case of a cross flow was performed and compared to their experimental results. The functional agreement was excellent, and their data correlate well with the following relationships:

$$Z^*_{\mathbb{C}} F_j = 2.1 F_0^{-1/3} S_\rho^{1/3} \tag{9}$$

$$X^*_{max}/F_j = F_0 \tag{10}$$

where $Z^*_{\mathbb{C}} \equiv Z' = Z_{\mathbb{C}}/r_0$ (at the plume centerline). Other measurements, including concentration distributions and longitudinal touchdown distances, were also reported.

On the basis of a very brief review by Ooms and Duijm (*18*), it would appear that the work of Anderson et al. (*14*) is of direct relevance. Unfortunately, the work was never published and a copy of their report has not been obtained. They used a water flume and varied θ between 45 and 90 degrees.

The response of a neutrally buoyant jet in a cross flow has been studied extensively. A summary to 1981 has been given by Crabb et al. (*19*). The characteristics of the jet deflection entrainment rates and mean turbulent flow properties have all been measured and documented. The observation of a double vortex structure in the downstream portion of the jet has intrigued investigators for years [see Abramovich (*20*) and Keffer and Baines (*21*)]. The interest lies both in the mechanism of generation and in the subsequent influence on the jet's boundary shape, trajectory, and entrainment rate.

In terms of numerical or analytical models of negatively buoyant jet or plume behavior, the survey by Hanna and Drivas (*22*), the volume edited by Britter and Griffiths (*23*), and the brief review by Ooms and Duijm (*18*) represent most of the currently available models and provide a comparative assessment of these models to the fairly small experimental data base.

DESCRIPTION OF THE EXPERIMENT

A tow tank was used to simulate the ambient flow. A round tube (the jet source) was towed through the tank at a constant

velocity. The use of a towing facility ensured a uniform, repeatable, and low turbulent mean flow (as seen by the jet or plume). The working fluid in the tow tank was water; the tank dimensions were 394 cm long by 40.6 cm wide and 50.8 cm deep. Salt water of various densities was used for the injection fluid. The water jet was mounted 10 cm above the bottom of the tank so that multiple test runs may be made with the same ambient fluid. The water jet was attached to a tow carriage that could be moved at a constant velocity along the tank's horizontal axis. The speed of the carriage could by varied between 0 and 12.4 cm/sec. The jet flux was controlled by a valve located between a constant head tank and the jet nozzle. The flow rate was measured by a tapered-tube flowmeter (calibrated for the variation in the fluid density). The resulting jet behavior was recorded photographically with two cameras, located at the side and end of the tank. The side camera used a shadowgraph technique to record the projected image of the jet (or plume) density structure on an opaque grid surface. The end camera recorded an illuminated slice of the jet that was produced by directing a sheet of light from the side of the tank and using a small amount of white tempera paint in the jet solution. Examples of the images recorded by this technique are shown in Figures 2–4.

The experimental program consisted of 260 separate tests. The ranges of the experimental parameters used in these studies follow:

Parameter	*Range of Values*
V_j	80–280cm/s
U_0	0–12.4 cm/s
θ	30°–90°
$\Delta\rho/\rho_j$	0.01–0.20
r_0	0.046–0.24 cm
Re_j	870–9220
Re_0	0–700
F_j	12–170
F_0	0–15

The values of the Reynolds numbers are based on jet diameter.

A typical experiment began with the installation of a selected nozzle at a predetermined angle setting. The tow tank was then filled and allowed to reach thermal equilibrium with the laboratory overnight. The vertical temperature structure was measured prior to testing. Thermal stratification within the tank never exceeded 2°C/m, so that internal wave motion and stratification within the tank were not important. Approximately 2 L of water in the tank temperature was placed in the constant head tank. Sodium chloride was added to the water in this supply tank until the desired jet density was reached. Density was determined with a hand-held refractometer. A small amount of white tempera paint was then added to the mixture in negligible amounts to affect the density. A series of tests at various towing speeds and jet velocities was then made, without the necessity to drain the tank. The tow tank density was monitored during these tests to ensure that the tank density above the level of the jet remained unstratified.

Photographic enlargements of the side and end views were made for each run. Measurements of the various length scales were then made from the photographs. A single operator

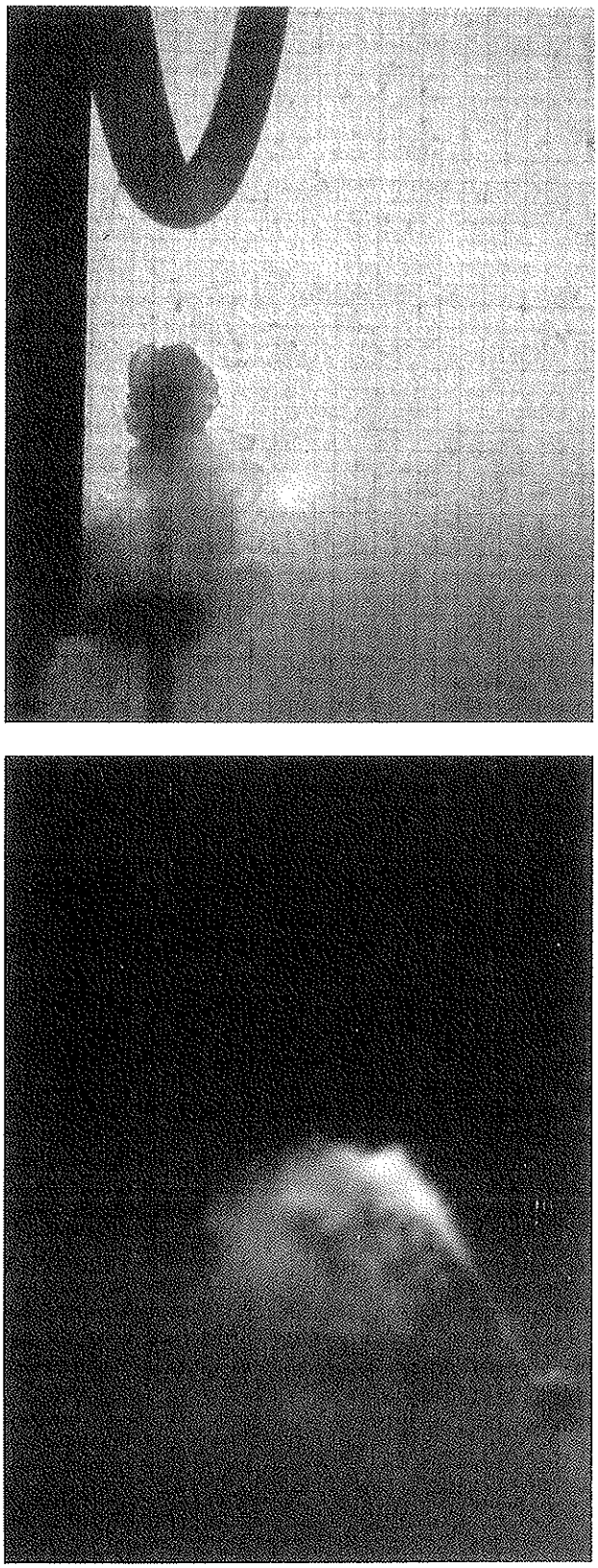

FIGURE 2 Side (*top*) and end (*bottom*) views of a jet (or plume) for the case of negligible cross flow; F_j = 25.2, F^0 = 0, Y^* = 67.2, Z^* = 60.2, θ = 60 degrees. The grid in the side (shadowgraph) image is 1 cm square.

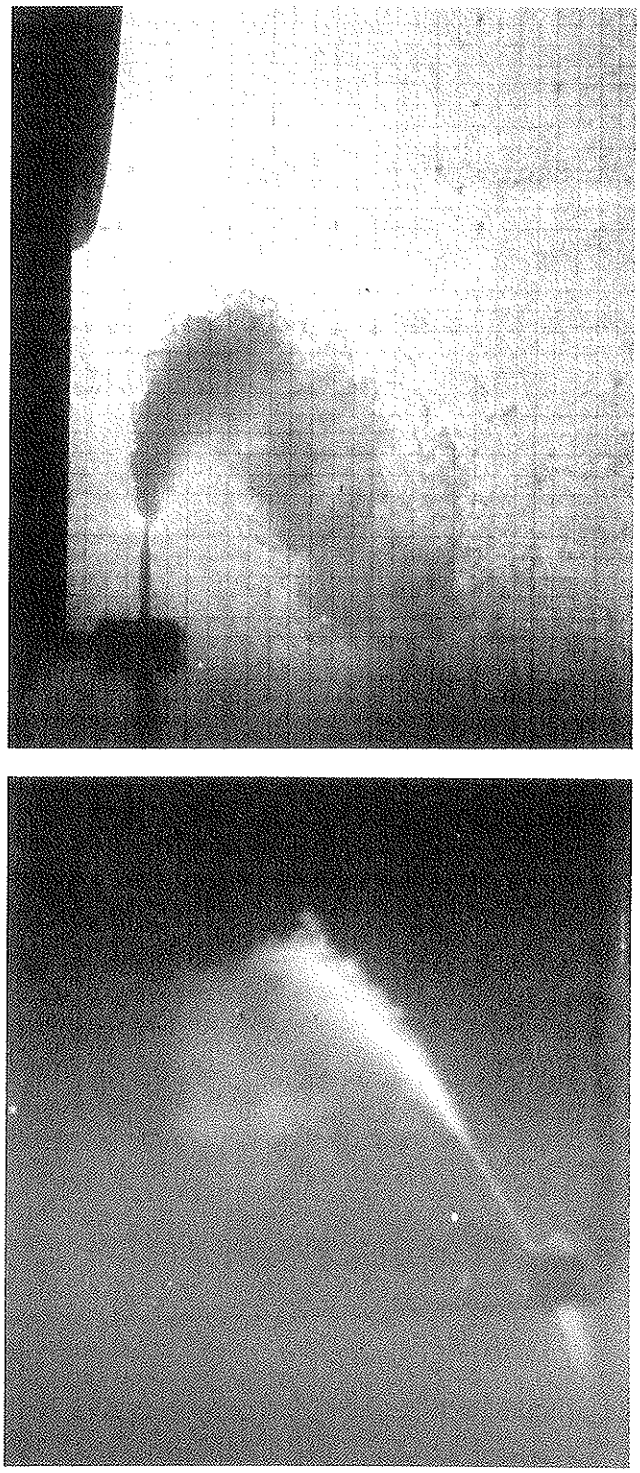

FIGURE 3 Side (*top*) and end (*bottom*) views of a jet (or plume) for the case of weak cross flow; F_j = 28.9, F_0 = 0.51, X^* = 34.9, Y^* = 54.6, Z^* = 81.3, θ = 60 degrees.

performed all of the measurements. In order to provide a check on any bias this procedure may have imposed, random tests were chosen and independent measurements of the length scales were made by a second observer. There was good agreement between the two estimates of these length scales.

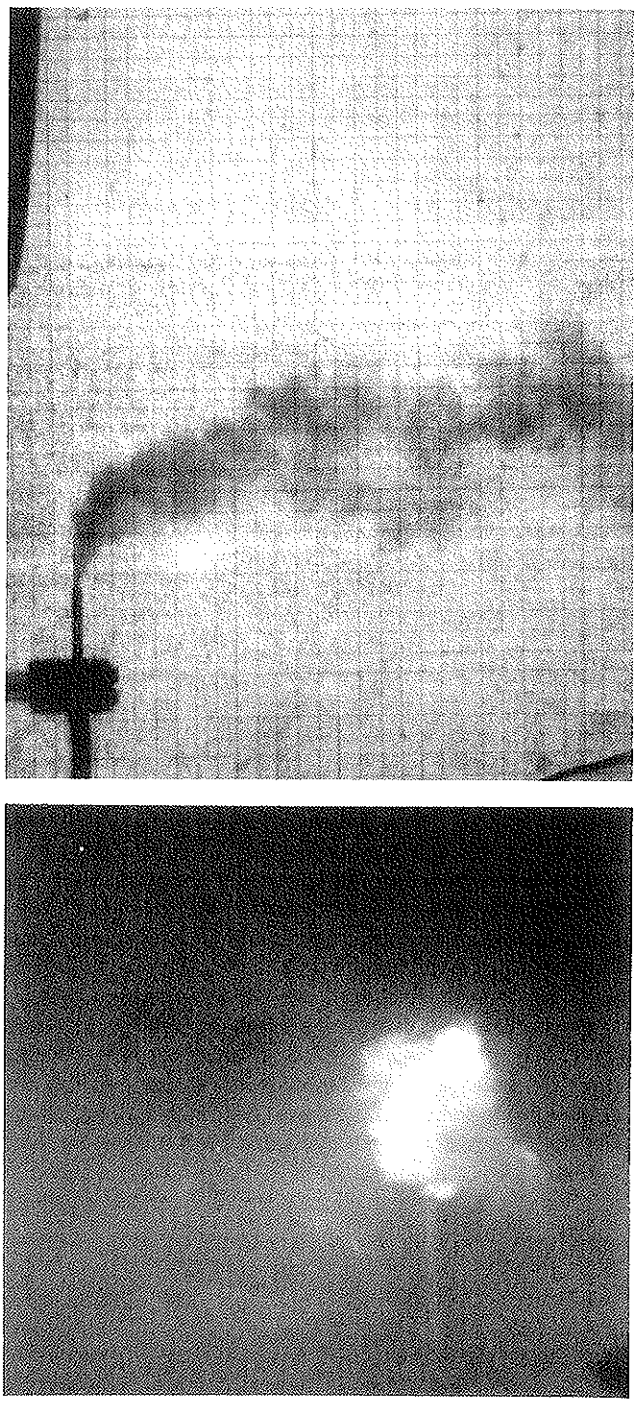

FIGURE 4 Side (*top*) and end (*bottom*) views of a jet (or plume) for the case of strong cross flow; F_j = 84.5, F_0 = 5.5, X^* = 179.0, Y^* = 67.0, Z^* = 95.0, θ = 60 degrees.

A summary of the experimental uncertainties in these measurements follows:

Parameter	*Uncertainty (%)*
F_j	9.1
F_0	2.4
L^*	9.6
L^*/F_j	13.3

However, the major source of scatter in the data is the inherent convoluted shape of the instantaneous boundary of the jet or plume. The instantaneous structure is captured in the photographs, not the average boundary shape, which would require averages over a number of observations.

EXPERIMENTAL RESULTS AND OBSERVATIONS

Observations

A complete photographic record of all tests has been obtained. Examples of these photographs are shown in Figures 2–4. These three photographic pairs are for the three ranges of F_0 applicable to negligible, weak, and strong cross flows, respectively.

The observed variability in all length scales increased at low F_0 and at the higher values of θ. Under these conditions, the plume length scales were observed to fluctuate with time around a mean value. These fluctuations were of the order of ± 20 percent of the mean length scales, while at the same time, the jet flow rates were observed to be constant. These low-frequency fluctuations are then a result of the interaction of the jet or plume with the column of fluid that is falling back around the upward-directed flow. At the lower angles and higher values of F_0, this interaction was not as pronounced or did not occur, and the variability in these length scales was much smaller. The highly convoluted entraining interface of these jet or plume flows is also quite apparent in these photographs, where the large-scale turbulent motion imposes a highly irregular boundary between the jet or plume fluid and the surrounding lower-density fluid. The difficulty of determining the mean interfacial length scales from a single photograph is apparent, and the scatter of the measurements is caused predominantly by this convoluted structure.

The double vortex structure mentioned earlier is shown in the photograph in Figure 5. This situation entailed a strong cross flow ($F_0 > 1$). The darker fluid on the inside of the double vortex was unmarked external fluid that was being entrained in a preferential way by this vortical structure. The photograph also shows the elliptical cross-sectional shape of the plume, whose minor axis is aligned in the same general direction as the initial jet angle. The entrainment processes observed are in sharp contrast to the turbulent interfacial entrainment processes of negligible or weak cross flow jets and plumes.

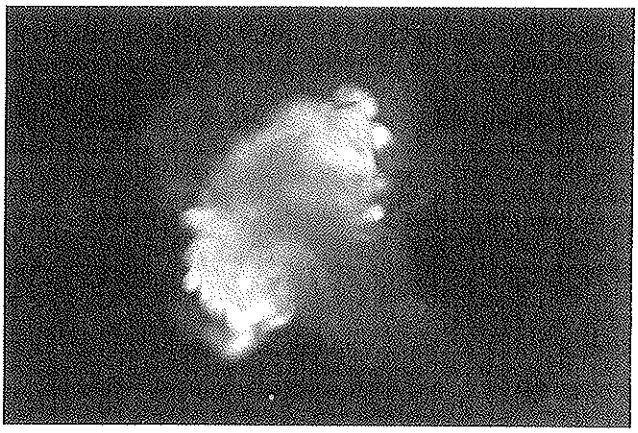

FIGURE 5 Double vortex structure, as seen from an end view; $F_j = 51$, $F_0 = 4.0$, $\theta = 60$ degrees.

Quantitative Results

Comparisons with Previous Work

The special case $\theta = 90$ degrees has, as has been noted, some limited prior research history. In Turner's (*9*) work, for $F_0 = 0$, a principal result was Equation 6. Figure 6 shows the data for $\theta = 90$ degrees and $F_0 = 0$ for the present study, along with Equation 6. The best fit line for these data (on the basis of eight tests) is

$$Z^* = 3.7F_j \tag{11}$$

which is 11 percent lower than that predicted by Equation 5 or the results of Hoot et al. (*12*). The observed fluctuations of the plume for high θ and low F_0 provide some explanation for this discrepancy. The maximum plume height excursion was not recorded (unless by chance), and a small number of instantaneous photographs were obtained. This procedure resulted in effective plume heights that varied over the range of instantaneous plume heights. Given a sufficiently large set of observations, the data then reflected the average plume height, rather than the maximum observed height. For these observations, a consistently lower value by 10 percent would then be expected. For the case of finite F_0, some visual averaging of the photographs was performed, to remove some of the instantaneous large-scale excursions form the data. This procedure is in contrast to the time lapse photographs used by Hoot et al. (*12*). The effect of such a procedure would be to record the maximum excursion over the time duration of the photograph.

A direct comparison with the data of Hoot et al. (*12*) for the case of finite F_0 is also possible. This comparison is shown in Figure 7, where the present data are plotted along with Equation 7 over the range of the experimental data used to

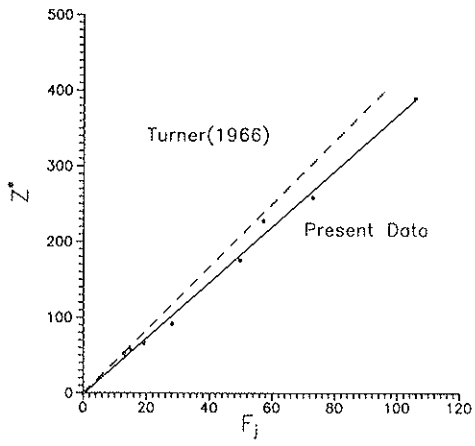

FIGURE 6 Comparison of vertical jet (or plume) behavior for no cross flow, with the results of Turner (*9*).

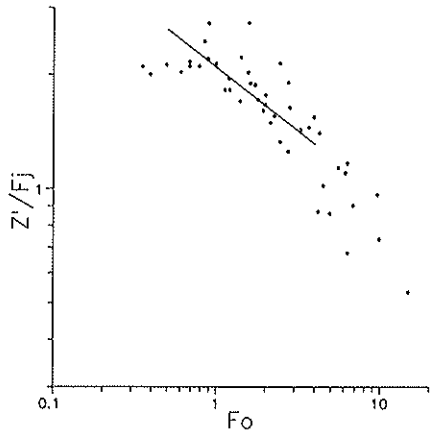

FIGURE 7 Comparison of vertical jet (or plume) behavior in a cross flow with the results of Hoot et al. (*12*). Equation 7 is shown as a solid line, over the limits of the experimental data.

obtain the correlation. The low-F_0 data of Hoot et al. were consistently below their reported asymptotic curve, in agreement with the present notion of a transition for $F_0 = 1$, as is discussed in the following sections.

Data Correlations

The measurements of the maximum vertical excursion of the plume Z^*, as a function of F_j, F_0, and θ will be discussed in detail. Many of the features of the jet or plume behavior are apparent from these observations alone. The other scales will then be presented and briefly discussed.

Maximum Plume Rise, Z^* There is an ambiguity in the interpretation of the definition of maximum plume rise when F_0 is varied continuously from 0 to values of the order of 15. For weak (or negligible) cross flows ($F_0 < 1$), the only observable is the maximum plume top, as the plume descends in the near vicinity of the initiating jet. This definition of plume rise was used in the previous subsection for the $F_0 = 0$ case study. For strong cross flows (i.e., $F_0 > 1$), the plume is advected in the downstream direction, so that a plume centerline may be considered. The example comparison study for finite F_0 in the previous section used such a definition. The two ways to define Z_{max} are not consistent, but may be related as

$$Z' \equiv Z_{max,\mathbb{C}} = Z_{max,top} - W/2 \tag{12}$$

for $F_0 > 0$. For negligible cross flow, the exact interpretation of $Z_{max,\mathbb{C}}$ is not clear, because the internal dynamics of an ascending jet (or plume) and the subsequent annular descending flow are not easily reduced to a single vertical length scale. The choice of the definition of Z_{max} for the data to be presented is

$$Z_{max} = Z_{max,top} \tag{13}$$

This choice was for reasons of consistency, so Z_{max} is defined the same for $F_0 < 1$ and for $F_0 > 1$. Additionally, the experimental techniques used required separate determinations of $Z_{max,top}$ and W_{max}. The increased uncertainty of combining these measurements is avoided by this choice. (Such increased experimental uncertainty is in evidence in Figure 7.)

Logarithmic plots of Z^*/F_j versus F_0 are shown in Figure 8(a–d). The dimensional arguments leading to Equation 2 are seen to be valid representations of the processes involved, as the data are reasonably well correlated. There is a definite change in the functional behavior of Z^*/F_j in the neighborhood of $F_0 \sim 1$, which marks the transition between weak and strong cross flows.

For the $F_0 = 0$ cases, $Z^*/F_j = f_{z,0}(\theta)$. The values of this angular dependence for $F_0 = 0$ were determined from a regression analysis of Z^* versus F_j, as was shown in Figure 6. The linear dependence of Z^* on F_j was consistent for all cases. The weak cross flow ($F_0 < 1$) behavior is essentially $Z^*/F_j \sim f_z(\theta)$, which is consistent with the scaling arguments leading to Equation 2. For $F_0 < 1$, $l_b < l_m$, so the transition to a pure plume would be expected before the effects of a cross flow became important. For $F_0 > 1$, the slope of the data in the form

$$Z^*/F_j = f_z(\theta)F_0^n \tag{14}$$

was also determined from a regression analysis. A summary of the results of these correlations follows:

Initial Jet Angle, θ *(degrees)*	$f_{z,0}(\theta)$	$f_z(\theta)$	n_z
90	3.70	3.61	−0.53
60	2.46	3.01	−0.59
45	1.76	2.53	−0.53
30	1.47	2.14	−0.50

A comparison of the values of $f_{z,0}(\theta)$ and $F_z(\theta)$ indicates that as θ decreases from 90 degrees, the value of $f_{z,0}(\theta)$ decreases much faster than $f_z(\theta)$. A plausible explanation for this behavior is the observed change in the interaction of the descending fluid with the rising central column of fluid. Comparison photographs of this process indicate that the interference of the descending fluid on the jet (or plume) decreases for $F_0 > 0$, where the low-momentum descending fluid is advected by the cross flow. Without this sweeping away of this descending fluid, the rising and falling fluid interaction is stronger, both by increasing the mixing rate within the plume and by an increased momentum exchange between the two flows.

The asymptotic analysis of Lindberg and Petersen (*1*) yielded a scaling for Z^*/F_j for the case of a jet with weak cross flow (i.e., $F_0 < 1$) and $\theta < 90$ degrees. The experimental values of $f_z(\theta)$ agree with the following equation to within 4 percent.

$$Z^*/F_j = f_z(\theta) = 2.3\,[(\sin\theta)(1 + \sin^{1/2}\theta)]^{1/2} \tag{15}$$

As would be expected, the values of $f_{z,0}(\theta)$ do not correlate well with this expression, in which it is noted that the entrainment hypothesis used in the analysis is only consistent with weak crossflow behavior.

Transverse Distance, Y^* Y^* is defined as Y_{max}/r_0, where Y_{max} is the measured maximum transverse distance of the jet

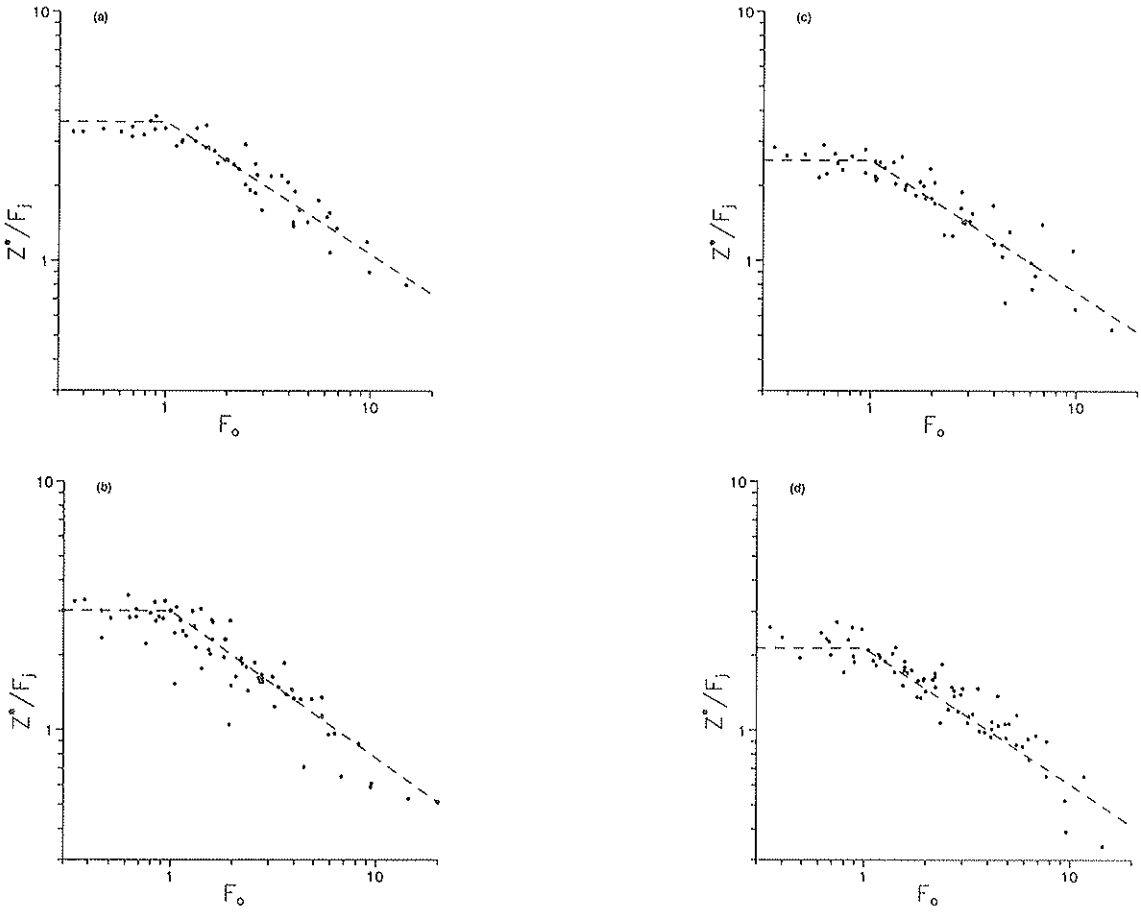

FIGURE 8 Dimensionless maximum plume rise, Z^*/F_j, in a cross flow as a function of cross flow Froude number, F_0; (a) θ = 90 degrees, (b) θ = 60 degrees, (c) θ = 45 degrees and (d) θ = 30 degrees.

(or plume) at the same location as Z_{max}. Figures 9(a–c) shows the measured Y^*/F_j values as a function of F_0. The asymptotic behavior of Y^*/F_j with F_0 is similar to the Z^*/F_j data of Figure 8. Adequate representations of this data are thus:

$$Y^*/F_j = \begin{cases} f_{y,0}(\theta) & \text{for } F_0 = 0 \\ f_y(\theta) & \text{for } 0 < F_0 < 1 \\ f_y(\theta) F_0^n & \text{for } F_0 > 1 \end{cases} \quad (16)$$

A data correlation summary of the linear regression analysis results for Y^* behavior (in which Y^* is zero for θ = 90 degrees) follows:

Injection Angle θ *(deg)*	$f_{y,0}(\theta)$	$f_y(\theta)$	n_y
90	—	—	—
60	1.7	1.7	−0.51
45	1.6	2.2	−0.59
30	3.0	2.7	−0.62

With the exception of $f_{y,0}$(45degrees), both $f_{y,0}$ and f_y increase with decreasing θ. The dependence of Y^*/F_j on F_0 continues to have an approximate $F_0^{-1/2}$ behavior, although the calculated slopes are even more negative.

Analysis of end view photographs of plume behavior subsequent to the maximum plume rise location indicates that Y does not appreciably increase further downstream. The initial y-momentum has become so diffuse through entrainment at this point that further transverse transport is small. For the present, then, Y^* may be assumed to be indicative of the maximum transverse plume distance, at least for $F_0 > 1$.

Longitudinal Distance, X^* The downstream location where Z_{max} occurs is defined as X_{max}. The scatter in the X^* data is significant for $F_0 > 1$ and illustrates the difficulty of determining X_{max} when the irregular plume boundary is essentially horizontal for a finite distance downstream. Within the limits of the data, an asymptotic equation of the form

$$X^*/F_j = f_x(\theta)\, F_0^n x \quad (17)$$

correlates the data for $F_0 > 0$. The following table summarizes the linear regression analysis for these data. Note that $X_{max} = F_0 = 0$.

Injection Angle θ *(degrees)*	$f_x(\theta)$	n_x
90	1.20	0.92
60	1.61	0.55
45	1.43	0.48
30	1.58	0.46

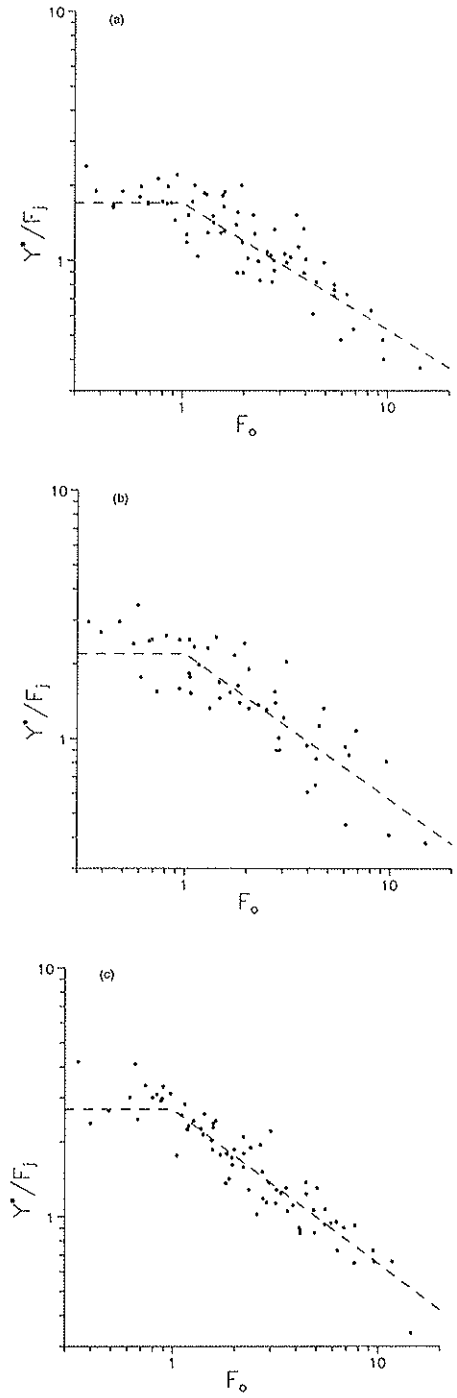

FIGURE 9 Dimensionless transverse length scale, Y^*/F_j, in a cross flow as a function of cross flow Froude number, F_0; (a) θ = 60 degrees, (b) θ = 45 degrees, and (c) θ = 30 degrees.

The variations of $f_x(\theta)$ are not significant; however, the comparison of n_x for θ = 90 degrees and all other angles is to be noted. The asymptotic theory of Hoot et al. (*12*) and Lindberg and Petersen (*1*), for θ = 90 degrees, predicts that $X^*/F_j \sim F_0$ (Equation 8), in agreement with the measurements. For θ < 90 degrees, this exponent, n_x, decreases by as much as a factor of two. A more detailed analysis will be necessary to clarify this observation; however, it is clear that the nature of the downstream plume trajectory changes when the initial jet angle is not vertical.

Plume Width Scale, W^* Observations off the plume width scale, W^*, were made a the Z_{max} location. These measurements were made from the side, by shadowgraphic images, so they represented the total vertical width of the plume at that location. Because of the elevation of the injection jet above the bottom of the tow tank, some measured widths exceed Z_{max}; however, these data were retained.

The following table summarizes the regression analysis for the four angles for $F > 1$, for the same asymptotic forms as Equation 12. The similar values of $f_w(\theta)$ and n_w for the various injection angles indicate that the vertical plume widths, for all injection angles, are similar. If a conceptual elliptically shaped plume in the downwind direction is used, the lower injection angles have a smaller Z_{max}, but a larger projected plume width, because of the tilting of the ellipse.

Injection Angle θ *(degrees)*	$f_w(\theta)$	n_w
90	2.5	−0.54
60	2.2	−0.61
45	2.2	−0.55
30	2.2	−0.55

APPLICATION TO SNOW PLUME BEHAVIOR

In terms of predicting snow plume cast distance or plume height for snowplow applications, Equation 12 can be rewritten as follows:

$$L_i^* = \eta f_i(\theta) F_0^{n_i+1} \tag{18}$$

for values of $F_0 < 1$, which is appropriate for most displacement plowing operations. Note that the length scales depend linearly on the moldboard efficiency, η.

Because nominal values of n_i for Y^* and Z^* are of the order of −0.5, the exponent on F_0 in Equation 18 is of the order of +0.5, in sharp contrast to the squared exponent of Equation 5. The characteristic length scale for these laboratory studies has been the nozzle radius r_0. An equivalent circular length scale for the case of a snow plume yields the following scale:

$$r_{0,e} = (A_{exit}\pi)^{1/2} = (bH/\pi\eta\alpha)^{1/2} \tag{19}$$

where b and H are the width and depth of the plowed snow, respectively, and α is the ratio of the final to initial snow densities. This equivalent scaling is limited to plow flow exit areas, which are approximately circular (or elliptical).

Example predictions of cast distance, Y_{max}, and maximum cast height, Z_{max}, using Equation 18, are shown in Figures 10 and 11. The assumed parameters for these calculations are snow depth, H = 0.20 m; plow width, b = 3.3 m; snow density, ρ_s = 100 kg/m^3; plow efficiency, η = 1.0; plow angle, φ = 0 degrees, and effective exit radius, $r_{0,e}$ = 0.46 m. Figure 10 also shows the prediction of cast distance using Equation 5 with the estimate of η_d as suggested by Shalman (*5*) for the case of θ = 45 degrees.

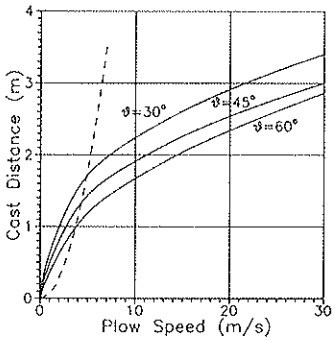

FIGURE 10 Predicted cast distance as a function of plow speed and initial moldboard exit angle, θ. The example parameters are summarized in the text. The dashed line is Equation 5, for θ = 45 degrees.

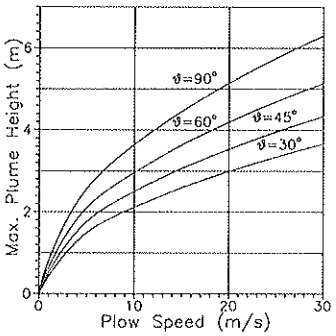

FIGURE 11 Predicted snow plume case height for the same parameters as in Figure 10.

The calculations are presented to illustrate the potential benefit of the current research in exit plume behavior. The current limitations on the parameters examined to date should be kept in mind.

SUMMARY AND CONCLUSIONS

The results of an experimental research program on the behavior of negatively buoyant jets (or plumes) are summarized in this paper. The effects of initial jet angle and cross flow have also been investigated.

Plume trajectory behavior, in the form of coordinate length scales at the location of maximum plume height, was determined from photographs of the visualized plumes. These length scales are functions of jet angle, θ, and the two Froude numbers: F_j and F_0. To the accuracy of the observations, the results have been correlated to an asymptotic power law as a function of flow regime in the form

$$\mathbf{L}^*/F_j = \begin{cases} f_{0,i}(\theta) & \text{for } F_0 = 0 \\ f_i(\theta) & \text{for } 0 < F_0 < 1 \\ f_i(\theta)F_0^{n} & \text{for } F_0 > 1 \ (F_0 > 0 \text{ for } X^*) \end{cases} \quad (20)$$

The flow regimes of $F_0 = 0$ (no crossflow), $0 < F_0 < 1$ (weak crossflow), and $F_0 > 1$ (strong cross flow) exhibit significantly different dynamical behavior, as is seen in the experimental observations and in the length scale results.

This study has successfully demonstrated the usefulness of using a water tow tank for the present jet (or plume) research. The range of parameters attainable in this facility has allowed for a clarification of the distinct flow regimes that have been discussed. Observations and photographic records have revealed much of the detail of these jet (or plume) flows from a variety of view angles.

At the outset of this phase of the study, the primary objectives were to

- Examine the effects of injection angle and cross flow on jet (or plume) behavior and relate the observations to previous work.
- Attain a wide range of parameter values to demonstrate the validity of the scaling analysis, and
- Determine the parameter space that may be identified with the various asymptotic flow regimes.

Within the limits of a photographic study, a large range of parameter space, and a relatively small number of tests, the objectives of the study have been met.

Further laboratory study will be directed toward the following objectives:

- Study the effect of changes in the exit jet geometry on jet (or plume) behavior, with emphasis on the strong crossflow regime;
- Include the azimuthal angle to study the effect of both fore and aft injection angles;
- Investigate the non-Boussinesq effect of S_ρ significantly different than 1, by using different solutes and suspensions;
- Examine the interaction between adjacent objects and the downstream plume behavior; including the incorporation of flow control devices attached to the adjacent structures;
- Compare jet (or plume) behavior in a quiescent flow to a turbulent environment; and
- Extend the analytical work to include higher level numerical models, primarily integral-based models.

ACKNOWLEDGMENTS

The research described herein was supported by the Strategic Highway Research Program (SHRP). SHRP is a unit of the National Research Council that was authorized by Section 128 of the Surface Transportation and Uniform Relocation Assistance Act of 1987. The authors would like to express their appreciation to Wayne Foslien, Jeff Rogers, and Roland Miller for their help with the data reduction and to R. N. Meroney of Colorado State University.

REFERENCES

1. W. R. Lindberg and J. D. Petersen. *The Negatively Buoyant Jet/Plume in an Ambient Cross Flow*. Fluid Mechanics Technical Report FMTR-90-1, Department of Mechanical Engineering, University of Wyoming, 1990.

2. H. B. Fischer, E. J. List, R. C. Y. Koh, J. Imberger, and N. H. Brooks. *Mixing in Inland and Coastal Waters*, Chapter 9, Academic Press, New York, 1979.
3. L. D. Minsk. Snow Removal Equipment. In *Handbook of Snow*, D. M. Gray and D. H. Male, eds., Pergamon, New York, 1981, pp. 648–670.
4. G. A. Vinnicombe. *Comparative Tests on Model Vee Snow Ploughs*. Report LR 180, Road Research Laboratory, Crowthorne, Berkshire, U.K., 1968.
5. D. A. Shalman. *Snowplows, Construction, Theory and Design*, 2nd ed. (in Russian). Mashinostroenie, Leningrad, U.S.S.R., 1973.
6. E. J. Hopfinger and P. Beghin. Buoyant Clouds Appreciably Heavier Than the Ambient Fluid on Sloping Boundaries. *Proc., 2nd International IAHR Symposium on Stratified Flows*. Troudheim, Norway, 1980, pp. 495–504.
7. E. J. Hopfinger. Snow Avalanche Motion and Related Phenomena. *Annual Reviews of Fluid Mechanics*, Vol. 15, pp. 47–76.
8. F. T. Bodurtha. The Behavior of Dense Stack Gases. *Journal of Air Pollution Control Association*, Vol. 11, 1961, pp. 431–437.
9. J. S. Turner. Jets and Plumes with Negative or Reversing Buoyancy. *Journal of Fluid Mechanics*, Vol. 26, 1966, pp. 779–792.
10. F. M. Holly and J. L. Grace. Model Study of Dense Jets in Flowing Fluid. *Journal of Hydraulics Division, ASCE*, Vol. 98. No. 9365, 1972, pp. 1921–1933.
11. A. B. Pincince and E. J. List. Disposal of Brine into an Estuary. *Journal of the WPCF*, Vol. 45, No. 11, 1973, pp. 2335–2344.
12. T. G. Hoot, R. N. Meroney, and J. A. Peterka. *Wind Tunnel Tests of Negatively Buoyant Plumes*. Report CER73-74TGH-RNM-JAP-13, Fluid Dynamics and Diffusion Laboratory, Colorado State University, 1973.
13. T. G. Hoot and R. N. Meroney. The Behavior of Negatively Buoyant Stack Gases. *Proc., 67th Annual Meeting, APCA*, Denver, Colo., 1974.
14. J. L. Anderson, F. L. Parker, and B. A. Benedict. *Negatively Buoyant Jets in a Cross Flow*. Report 660/2-73-012, U.S. Environmental Protection Agency, 1973.
15. V. H. Chu. Turbulent Dense Plumes in Laminar Cross Flow. *Journal of Hydraulic Research*, Vol. 13, No. 3, 1975, pp. 263–279.
16. A. Badr. Temperature Measurements in a Negatively Buoyant Round Vertical Jet Issued in a Horizontal Cross Flow. In *Atmospheric Dispersion of Heavy Gases and Small Particles*, G. Ooms and H. Tennekes, eds., Springer-Verlag, New York, pp. 167–176.
17. R. N. Meroney. Wind Tunnel Experiments on Dense Gas Dispersion. *Journal of Hazardous Materials*, Vol. 6, Nos. 1–2, 1982, pp. 85–106.
18. G. Ooms and N. J. Duijm. Dispersion of a Stack Plume Heavier Than Air. In *Atmospheric Dispersion of Heavy Gases and Small Particles*. G. Ooms and H. Tenekes, eds., Springer-Verlag, New York, 1984, pp. 1–23.
19. D. Crabb, D. F. G. Duraõ, and J. H. Whitelaw. A Round Jet Normal to a Crossflow. *Journal of Fluids Engineering, Transactions of ASME*, Vol. 103, 1981, pp. 142–153.
20. G. N. Abramovich. *The Theory of Turbulent Jets*. Chapter 12, MIT Press, Cambridge, Mass., 1963.
21. J. F. Keffer and W. D. Baines. The Round Turbulent Jet in a Cross Wind. *Journal of Fluid Mechanics*, Vol. 15, 1963, pp. 481–496.
22. S. R. Hanna and P. J. Drivas. *Guidelines for Use of Vapor Cloud Dispersion Models*. American Institute of Chemical Engineers, 1987.
23. R. E. Britter and R. F. Griffiths. Dense Gas Dispersion. *Journal of Hazardous Materials*, Vol. 6, Parts 1 and 2, Elsevier, 1982.

This paper presents the views of the authors only, not necessarily the views of the National Research Council, of SHRP, or of SHRP's sponsors. The results reported are not necessarily in agreement with the results of other SHRP research activities. They are reported to stimulate review and discussion within the research community.

Publication of this paper sponsored by Committee on Winter Maintenance.